Journal of Photochemistry and Photobiology A: Chemistry 199 (2008) 188–196

Contents lists available at ScienceDirect

Journal of Photochemistry and Photobiology A: Chemistry

journal homepage: www.elsevier.com/locate/jphotochem

Molecular construction and photophysics of luminescent covalently bonded hybrids by grafting the lanthanide ions into the silicon–oxygen networks and carbon chains

Xiaofei Qiao[a], Bing Yan[a,b,*]

[a] Department of Chemistry, Tongji University, Siping Road 1239, Shanghai 200092, China
[b] State Key Laboratory of Rare Earth Materials Chemistry and Applications, Beijing 100871, China

ARTICLE INFO

Article history:
Received 2 January 2008
Received in revised form 10 April 2008
Accepted 17 May 2008
Available online 3 July 2008

Keywords:
Photophysical property
Covalently bonded hybrid material
Sol–gel
Organic chain and inorganic network

ABSTRACT

Through the hydrogen transfer nucleophilic addition reaction between the hydroxyl groups of the glycol, the diglycol or the polyglycol and the isocyanate groups of 3-(triethoxysilyl)-propyl isocyanate (TEPIC), the hybrid precursor G–Si, DG–Si and PG–Si were obtained. And then G–Si, DG–Si or PG–Si has coordinated to the rare earth ions with the carbonyl groups to form the three kinds of hybrid materials through hydrolysis and copolycondensation with the tetraethoxysilane (TEOS) via sol–gel process. The data in NMR, FT-IR and ultraviolet absorption spectra indicate that the effective precursors have been obtained successfully. Moreover, seen from the fluorescent excitation and emission spectra, TG plots and electronic microscopy diagraphs, respectively, the obtained materials have the excellent fluorescent intensities, outstanding thermal stabilities and regular and homogenous trunk stripes microstructures. Ulteriorly, the X-ray diffraction patterns were obtained under the room temperature to describe the structure of the materials.

1. Introduction

In recent years, a lot of attention has been paid to the inorganic–organic hybrid materials due to the unique and peculiar properties. Especially, the rare earth-containing hybrid material has played an important and prominent role in a variety of areas such as biology, dyestuff, fluoroimmunoassays [1,2], electroluminescence devices [3,4], and polymer optical fibers [5,6], as the result of the extremely sharp emission bands, long lifetime, potential high internal quantum efficiency, the extensive range of mechanical, chemical, optical and electronic properties of the hybrid material [7,8]. Considering that the f–f electronic transitions of the rare earth metal ions are forbidden and they have a low absorption coefficient in visible–ultraviolet region, in the system of the organic–inorganic hybrid material the organic ligand is introduced to absorb the light and transfers the energy to the emitting metal (rare earth metal ions), which is called antenna effect, to sensitize the metal ions, protect metal ions from vibrational coupling and increase the absorption cross-section [9]. Besides, since the lanthanide organic complex has the poor thermal stability and mechanical properties to restrict the practical application, while the inorganic host has better thermal stability and mechanical resistance but worse luminescent properties, the advantages have been enhanced and the weakness has been overcome through the combination of both together.

According to the interaction between the rare earth-containing organic component and the inorganic host of hybrid material, the hybrid material has been divided into two major classes by Sanchez and Ribot [10]. The organic and inorganic components combine with the weak interactions such as hydrogen bonding, van der waals force or weak static effects, so-called class I, while class II with the powerful chemical covalent bond [11–15]. In the class I, the two components have presented as two separate phases and the concentration quenching and the leaching effect of the photoactive molecules (rare earth ions) have occurred easily. Besides, the dopant concentration of rare earth organic complexes in inorganic matrix in class I is very low and it is difficult to obtain transparent and uniform material. Therefore, the major investigation has been absorbed in the development of class II hybrid material in recent years since it has exhibited monophonic appearance even at a high concentration of lanthanide complexes [16–25]. Moreover, the latter belong to the molecular-based composite materials and protect the emitting metal from agglomerating so as to make it more possible to modify the network structure and obtain other properties of novel multifunctional materials combining with different components through the chemical covalent bonds in a single phase [26].

Many kinds of methods to synthesize the hybrid materials have been invented and utilized in many areas. It is shown that the

* Corresponding author. Tel.: +81 21 65984663; fax: +81 21 65982287.
E-mail address: byan@tongji.edu.cn (B. Yan).

1010-6030/$ – see front matter © 2008 Elsevier B.V. All rights reserved.
doi:10.1016/j.jphotochem.2008.05.021

sol–gel method has become a suitable approach to prepare the novel luminescent hybrid materials due to its advantages in the operational process such as the low reaction temperature, the control on the final various shapes and so on [27,28]. Therefore, the rare earth-containing organic complexes are protected from moisture and high temperatures when incorporated into inorganic transparent matrices by sol–gel method [29]. Besides, the hybrid material synthesized by sol–gel method combine the thermal stability and the mechanical strength of silica with the optical characteristics of active organic rare earth complex, realizing the versatility in optical and mechanical properties by employing various kinds of the alkoxides. In order to combine the merits of the pure emission color of rare earth organic complex with the plastic properties of the polymer material, polymer-based rare earth hybrid materials have emerged recently [30–34]. Hybrid materials containing the high molecular weight polymer, such as poly(oxyethylene), and poly(oxypropylene), and metal salts have attracted plenty of interest in recent years due to their various practical applications as high energy density batteries, sensors, and electrochromic and photoelectrochemical solid-state devices [35–39].

In this paper, we have brought forward a novel synthetic approach to construct a series of lanthanide polymer-containing hybrid materials. We have modified the ligand glycol (diglycol and polyglycol) by employing 3-(triethoxysilyl)-propyl isocyanate (TEPIC) through the hydrogen transfer nucleophilic addition reaction, subsequently, the rare earth metal ions have coordinated with them by the carbonyl groups. Moreover, the last hydrolysis/polycondensation process has occurred between the derivatives from the ligand glycol (diglycol and polyglycol) to form the Si–O network by sol–gel method and obtain the lanthanide hybrid polymers with high molecule weigh and high luminescent intensities and homogenous microstructure.

2. Experimental

2.1. Physical measurements

Infrared spectroscopy were obtained in KBr pellets and recorded on a Nexus 912 AO446 FT-IR spectrophotometer in the range of 4000–400 cm^{-1}. Ultraviolet absorption spectra (5×10^{-4} mol L^{-1} chloroformic solution) and the ultraviolet–visible diffuse reflection spectra of the powder samples were recorded by an Agilent 8453 spectrophotometer and a BWS003 spectrophotometer, respectively. ^1H NMR spectra were recorded in deuterate DMSO by a Bruker AVANCE-500 spectrometer with tetramethylsilane (TMS) as internal reference. The fluorescent excitation and emission spectra were obtained on a PerkinElmer LS-55 spectrophotometer: excitation slit width = 3 nm, emission slit width = 5 nm. The fluorescence decay properties were recorded on an Edinburgh Analytical Instruments. The microstructure was estimated by scanning electronic microscope (SEM, Philips XL-30). The X-ray diffraction (XRD) measurements of the powdered sample were carried out by a BURKER

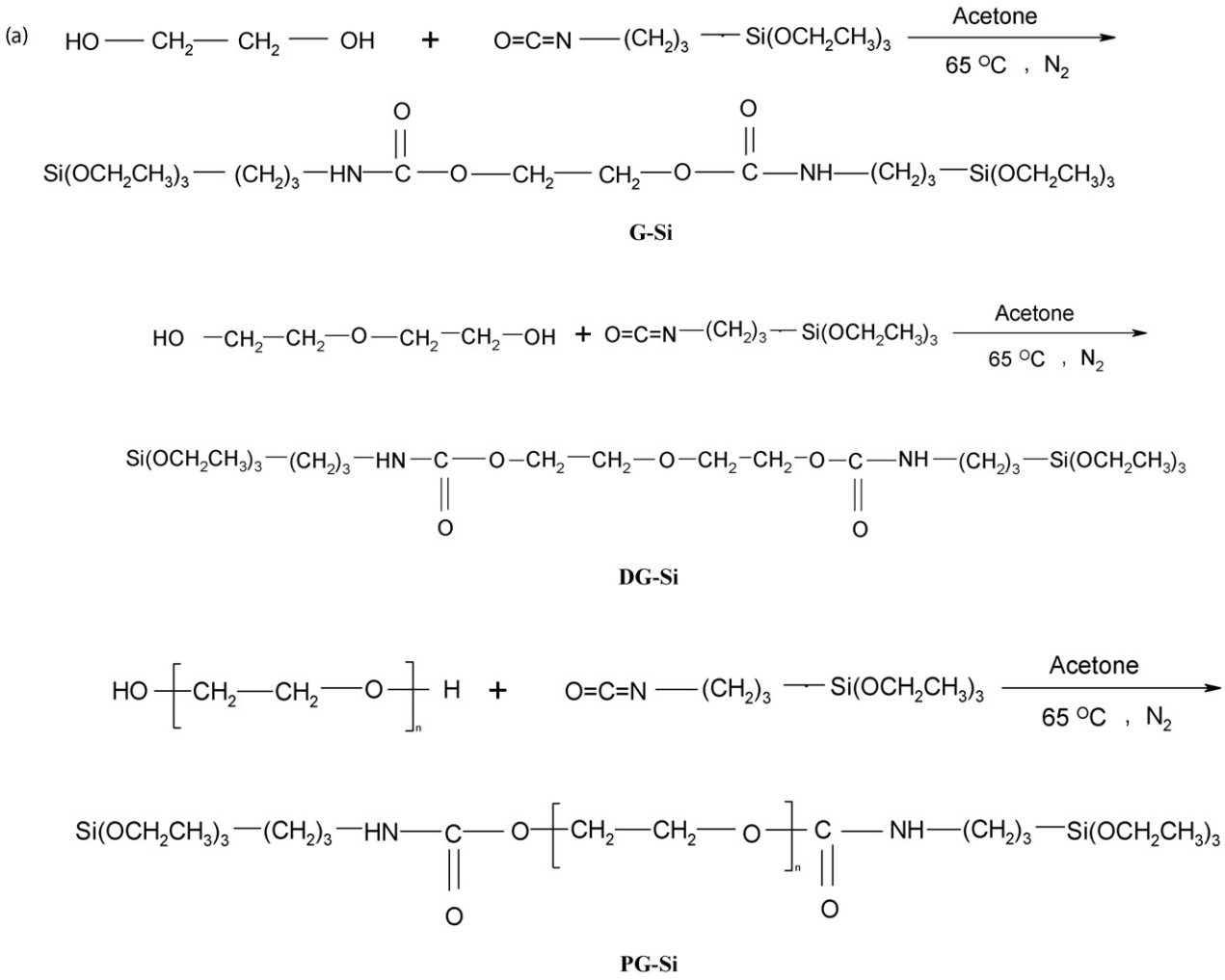

Fig. 1. Scheme of synthesis processes of the precursors (G–Si, DG–Si and PG–Si in a) and hybrid materials (DG–Si–RE, DG–Si–RE and PG–Si–RE in b).

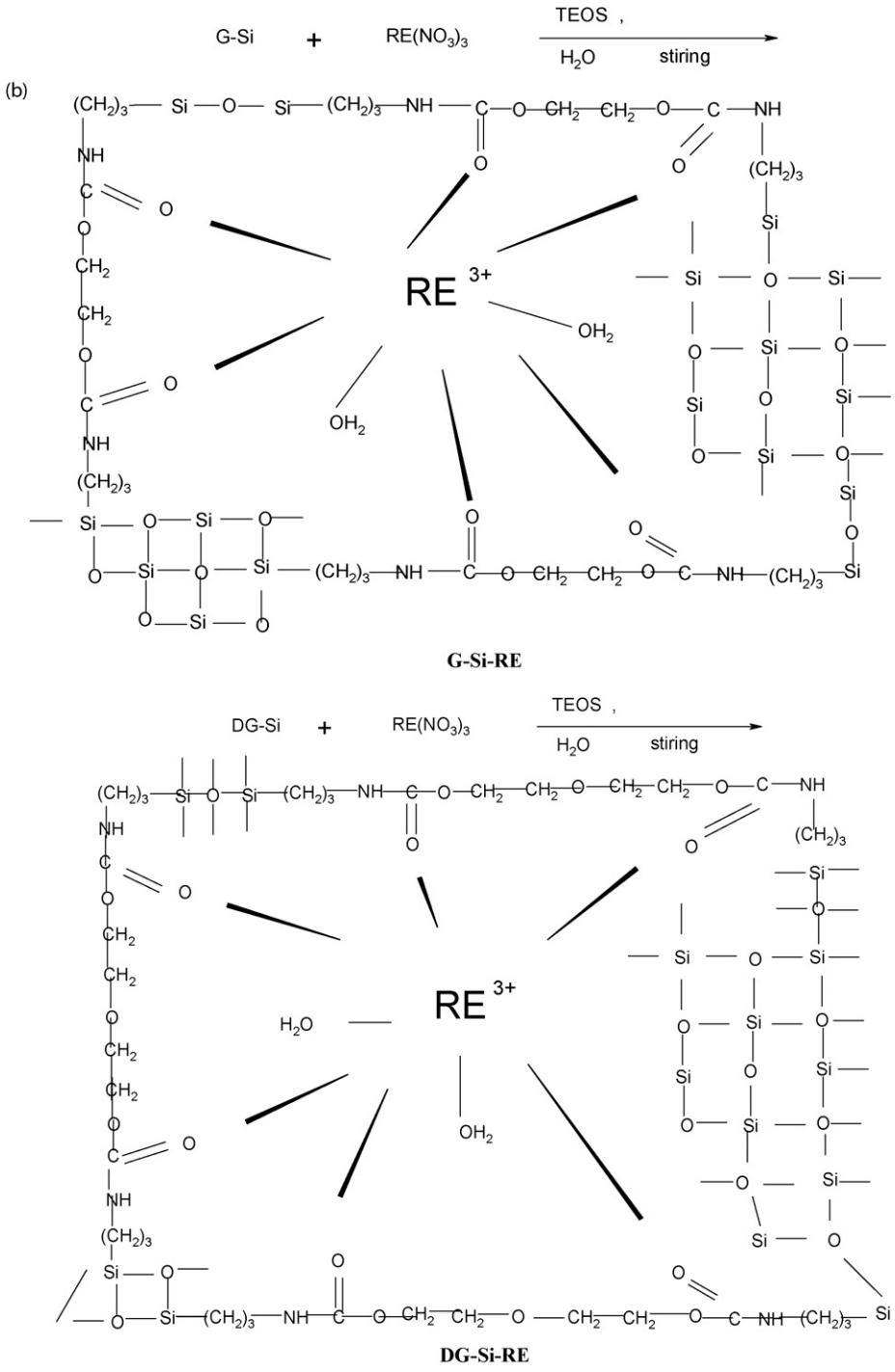

Fig. 1. (*Continued*)

D8 diffractometer (40 mA to 40 kV) using monochromated Cu Ka1 radiation (k = 1.54 Å) over the 2θ range of 10–70°. All measurements were completed under the room temperature. Thermogravimetry (TG) was obtained on Netzsch, model STA 409C in the following conditions: nitrogen air atmosphere, heating/cooling rate of 15 °C/min, 10.804 mg of powder; crucibles of Al_2O_3.

2.2. Chemicals

3-(Triethoxysilyl)-propyl isocyanate is supplied by Lancaster Synthesis Ltd. Glycol, diglycol and polyglycol are purchased from shanghai chemical plant. Other starting reagents are analytically pure.

2.3. Procedures

Synthesis of precursor (G–Si, DG–Si and PG–Si): 0.1 mol glycol, diglycol or polyglycol were dissolved in acetone solution completely by stirring, respectively, 0.1 mol 3-(triethoxysilyl)-propyl isocyanate was then added to the solution slowly. After refluxing at 45 °C under nitrogen for 12 h, the whole mixture was concentrated to remove the solvent acetone using a rotary vacuum evaporator, and the yellow slimy liquid was obtained. Subsequently, the decon-

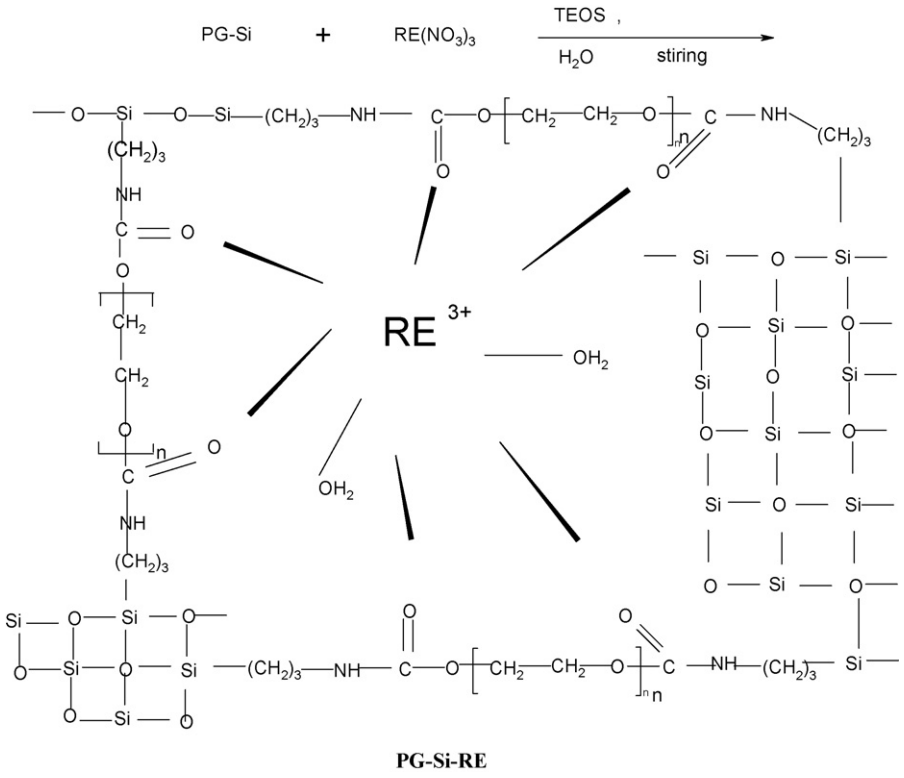

Fig. 1. (*Continued*).

tamination processes (precipitation and filtration) were carried on three times by employing the hexane solvent. At last the pure yellow liquid samples were obtained and dried in a vacuum (G–Si, DG–Si, PG–Si) (see Fig. 1a). The ^{1}H NMR data of DG–Si are as follows: δ 0.71(4H, t), 1.22(18H, t), 1.81(4H, m), 3.25(4H, m), 3.47(4H, t), 3.68(12H, m), 3.85(4H, t), 4.85(2H, t). The ^{1}H NMR data of PG-Si are as follows: δ 0.68(4H, t), 1.07(18H, t), 1.85(4H, m), 3.35(4H, m), 3.42(20H, t), 3.85(12H, m), 4.25(2H, t).

Synthesis of the lanthanide hybrid materials with Si–O networks and organic carbon chains (G–Si–RE, DG–Si–RE, PG–Si–RE): the precursor G–Si, DG–Si, PG–Si was mixtured in the absolute ethanol solution completely and a stoichiometric amount of $Tb(NO_3)_3{\cdot}6H_2O$ (0.32 g) or $Eu(NO_3)_3{\cdot}6H_2O$ (0.31 g) was added into the solution, respectively. After 3 h, tetraethoxysilane (TEOS) and H_2O were added into the mixture while stirring, and then one drop of diluted hydrochloric acid was added to promote hydrolysis. The molar ratio of $RE(NO_3)_3{\cdot}6H_2O$: G–Si (DG–Si, PG–Si): TEOS:H_2O was 1:3:6:24. (TEOS 0.45 mL, 0.833 g; H_2O 0.288 g). The mixture was agitated magnetically to achieve a single phase in a covered Teflon beaker, and then it was aged at 70 °C until the onset of gelation in about 5 days. The gels were collected as monolithic bulks and were ground into powdered material for the photophysical studies (G–Si–RE, DG–Si–RE and PG–Si–RE) (see Fig. 1b).

3. Results and discussion

3.1. FI-IR spectra

The Fourier transform infrared spectra of TEPIC, (A) G–Si and (B) DG–Si are shown in Fig. 2. From the Fourier transform infrared spectra of TEPIC, it is shown that there are four peaks at 2880–2975 cm^{-1} and 2265–2369 cm^{-1} indicating the existence of three methylene groups and the isocyanate groups (O═C═N), but there is no obvious peak at 1560–1690 cm^{-1}, which attribute to the bending vibration of the —NH— group. After the hydrogen transfer nucleophilic addition reaction to synthesize the precursors G–Si and DG–Si, from the Fourier transform infrared spectra it is shown that the peaks 1693 cm^{-1} (A) and 1695 cm^{-1} (B) indicate the emergence of the amide groups (CONH) and the three peaks have shifted to about 2973–2874 cm^{-1} in (A) and 2974–2878 cm^{-1} in (B) illuminate the existence of the three methylene groups, both suggesting that 3-(triethoxysilyl)-propyl isocyanate has been successfully grafted onto glycol and diglycol, respectively, through the hydrogen transfer nucleophilic addition reaction between hydroxyl group of glycol, diglycol and the isocyanate of 3-(triethoxysilyl)-propyl isocyanate. Moreover, the peaks at about 2250 cm^{-1} in A and B are assigned to the isocyanate group (—NCO) of unreacted TEPIC, since there is one possibility that the reaction time or temperature are not the most proper for the hydrogen transfer nucleophilic addition reaction, and we will continue do more research about the reaction conditions in the future. The peaks located at 1215 cm^{-1} and 1216 cm^{-1} in A and B are attributed to the stretching vibration (Si—C) and the broad peak at 1039–1147 cm^{-1} has emerged in A and B related to the stretching vibration of Si—O—C, which indicates the appearance of siloxane bonds, both of those also illuminate the success of the graft reaction of 3-(triethoxysilyl)-propyl isocyanate in harmony with the above conclusion. Moreover, it is found that no (Si—C) bond split occurred during the course of hydrolysis/polycondensation reactions. The wide band absorption at about 3400 cm^{-1} is the overlap of the asymmetric and symmetric stretch (H—O—H) in the crystal water (3600–3000 cm^{-1}), the double multiple absorption of C═O (3500–3400 cm^{-1}) and N—H (3500–3200 cm^{-1}) in A and B.

3.2. Photoluminescence spectra

The fluorescent excitation and emission spectra of the lanthanide hybrid materials are shown in Fig. 3. The excitation spectra were obtained by monitoring the emission of Tb^{3+} or Eu^{3+} ions at

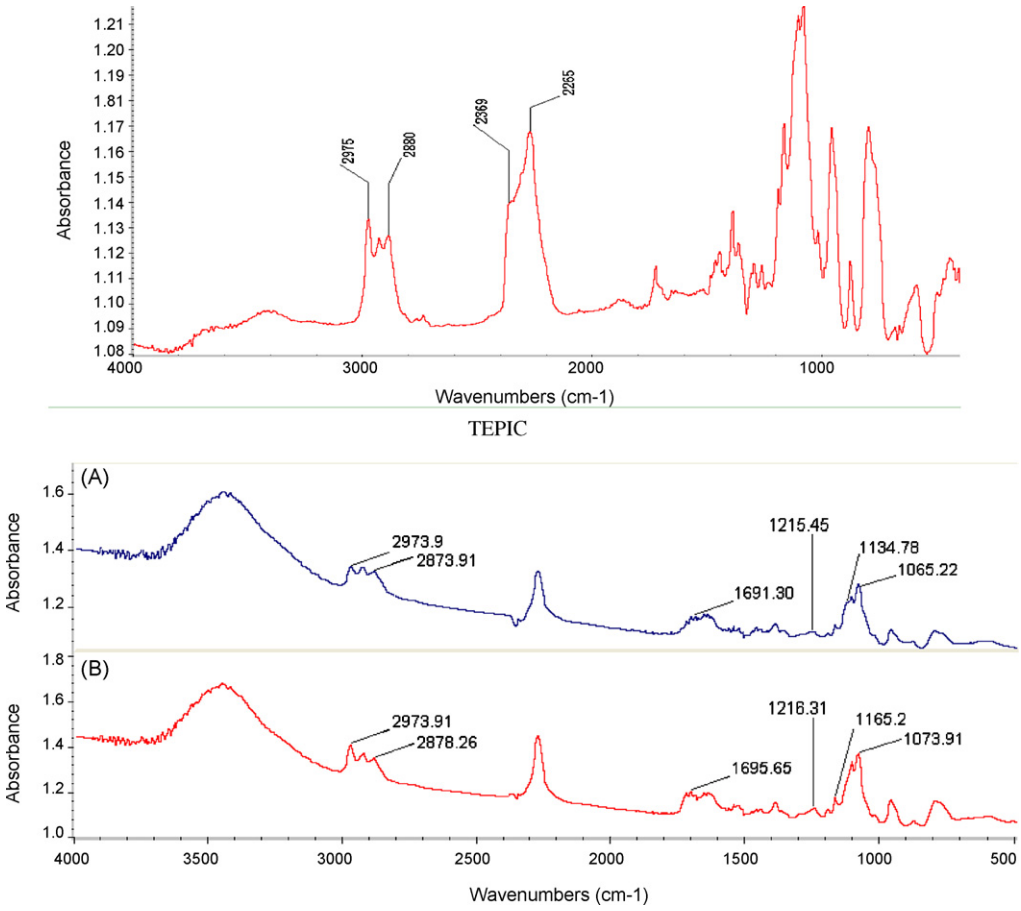

Fig. 2. The Fourier transform infrared spectra of the TEPIC and two precursors (A) G–Si and (B) DG–Si.

543 or 613 nm and dominated by a broad band centered at about 320–357 and a narrow peak centered at 393 nm, respectively, which are ascribed to the characteristic absorption of the lanthanide complexes arising from the efficient transition based on the conjugated double bonds of the carbonyl groups (C=O). As a result, the emission lines of the hybrid material were assigned to the transitions from the $^5D_4 \rightarrow {}^7F_J$ (J = 6, 5, 4, 3) transitions at about 486, 543, 583 and 619 nm for Tb^{3+} and $^5D_0 \rightarrow {}^7F_J$ (J = 1, 2, 3, 4) transitions at about 589 nm, 612 nm, 648 nm and 701 nm for Eu^{3+}, respectively. Observed from Fig. 3a, it is found that the green emission intensities are the strongest in all of emission of terbium complexes, which can be explained by the conclusion that the leaching of the photoactive molecules was avoided and a higher concentration of emitting metal ions was obtained. And seen form Fig. 3b among these emission peaks of the complexes of chelated Eu^{3+}, red emission intensities (arbitrary unit, a.u.) of electric dipole transition of $^5D_0 \rightarrow {}^7F_2$ at about 613 nm (392.7 for *a*, 237.0 for *b* and 270.9 for *c*) are all stronger than the orange emission intensities of magnetic dipole transition of $^5D_0 \rightarrow {}^7F_1$ at about 589 nm (219.7 for *a*, 183.9 for *b* and 209.8 for *c*), respectively, which indicate Eu^{3+} site in an environment without inversion symmetry [40]. Therefore, it is indicated that the effective energy transfer took place between the four precursors and the chelated rare earth ions. Other factors still cannot be excluded such as relatively rigid structure of silica gel which limits the vibration of ligand in the hybrid materials and prohibits non-radiative transitions. Accordingly, we may expect that through this efficient way, leaching of the photoactive molecules can be avoided, higher concentration of metal ions will be realized and clustering of the emitting centers may be prevented.

From the spectra (a) and (b), it is observed that the line of A gives stronger fluorescence than that of B and C in (a), while than b and c in (b), indicating the energy gap between the triplet state energy of G–Si and the resonant emissive energy level of the central irons Tb^{3+} and Eu^{3+} is smaller than that between the precursor DG–Si or PG–Si and Tb^{3+} and Eu^{3+}. The potential reason may be the PG–Si has the longer carbon chains than the others, which induces that the precursor PG–Si is difficult to coordinate to rare earth ions in this system. Following Dexter's exchange energy transfer theory [41]: the luminescence intensity of hybrid material depends on the matching degree of the ligand's triplet state energy and lanthanide iron's emission energy. Therefore, it is speculated that the energy matching degree between the resonant emissive energy level of Tb^{3+} and the triplet state energy of the precursors G–Si is the best in Fig. 3a, while in Fig. 3b the energy matching between the resonant emissive energy level of Eu^{3+} and the triplet state energy of the precursors G–Si is a litter more successful than others. Besides, on the basis of Sato's results [42], larger or smaller ϕE ($Tr–Ln^{3+}$) will have converse influences on both the rate constant of the intermolecular energy transfer k_{ET}[41] and the inverse energy transfer rate constant $k(T)$ [43]. Consequently, luminescence of rare earth ions is ineffective.

3.3. Luminescence decay times (τ) and emission quantum efficiency (η)

According to the emission spectrum and the lifetime of the Eu^{3+} first excited level (τ, $^5D_0$), the emission quantum efficiency (η) of the $^5D_0$ excited state can be determined as 566 μs. Assuming that

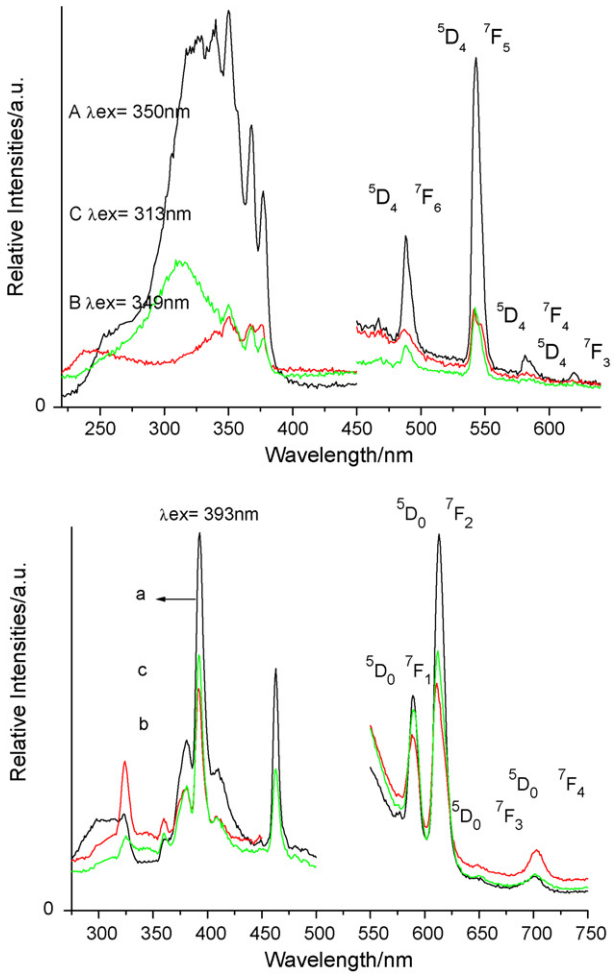

Fig. 3. The fluorescent excitation and emission spectra of the hybrid materials (A) G–Si–Tb, (B) DG–Si–Tb, (C) PG–Si–Tb in a, (a) G-Si-Eu, (b) DG–Si–Eu and (c) PG–Si–Eu in b.

only non-radiative and radiative processes are essentially involved in the depopulation of the $^5D_0$ state, η can be defined as follows [44]:

$$\eta = \frac{A_r}{A_r + A_{nr}} \quad (1)$$

Here, A_r and A_{nr} are radiative and non-radiative transition rates, respectively. A_r can also be obtained by summing over the radiative rates A_{0J} for each $^5D_0 \rightarrow {}^7F_J$ ($J = 0$–4) transitions of Eu^{3+}. The branching ratio for the $^5D_0 \rightarrow {}^7F_{5,6}$ transitions can be neglected as they are not detected experimentally, whose influence can be ignored in the depopulation of the $^5D_0$ excited state. Since $^5D_0 \rightarrow {}^7F_1$ belongs to the isolated magnetic dipole transition, it is practically independent of the chemical environments around the Eu^{3+} ion, and thus can be considered as an internal reference for the whole spectrum, the experimental coefficients of spontaneous emission, A_{0J} can be calculated according to the equation [45–47]:

$$A_{0J} = A_{01}\left(\frac{I_{0J}}{I_{01}}\right)\left(\frac{\nu_{01}}{\nu_{0J}}\right) \quad (2)$$

Here, A_{0J} is the experimental coefficients of spontaneous emission. A_{01} is the Einstein's coefficient of spontaneous emission between the $^5D_0$ and $^7F_1$ energy levels. In vacuum, A_{01} as a value of 14.65 s^{-1}, when an average index of refraction n equal to 1.506 was considered, the value of A_{01} can be determined to be 50 s^{-1} approximately

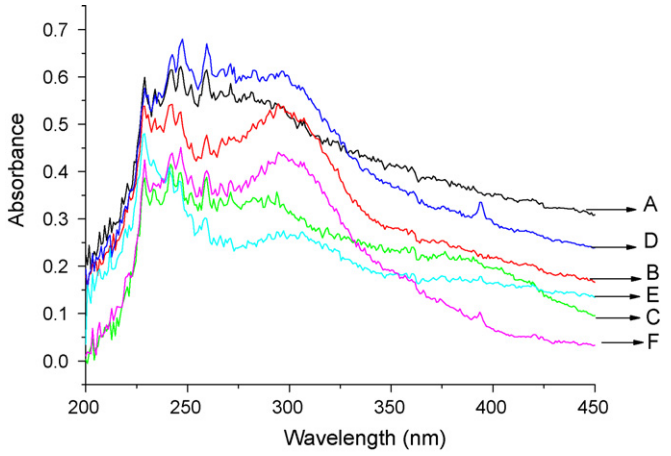

Fig. 4. The ultraviolet–visible diffuse reflection absorption spectra of the raw materials. (A) G–Si–Tb, (B) DG–Si–Tb, (C) PG–Si–Tb, (D) G–Si–Eu, (E) DG–Si–Eu and (F) PG–Si–Eu.

($A_{01} = n^3 A_{01(vac)}$) [48]. I_{01} and I_{0J} are the integrated intensities of the $^5D_0 \rightarrow {}^7F_1$ and $^5D_0 \rightarrow {}^7F_J$ transitions ($J = 0$–4) with ν_{01} and ν_{0J} ($\nu_{0J} = 1/\lambda_J$) energy centers, respectively. ν_{0J} refers to the energy barrier and can be determined from the emission bands of Eu^{3+}'s $^5D_0 \rightarrow {}^7F_J$ emission transitions. The emission intensity, I, can be taken as integrated intensity S of the $^5D_0 \rightarrow {}^7F_{0-4}$ emission curves. On the basis of Refs. [49–53], the value of $A_{01} \approx 50\ s^{-1}$ and the lifetime (τ, 566 μs), radiative (A_r, 151 s^{-1}), and non-radiative (A_{nr}, 1617 s^{-1}) transition rates are related through the following equation:

$$A_{tot} = \frac{1}{\tau} = A_r + A_{nr} \quad (3)$$

On the basis of the above discussion, the quantum efficiency of the he hybrid material G–Si–Eu can be determined as 8.54%. From the equation of η, it can be seen the value η mainly depends on the values of two quantum: one is lifetime and the other is I_{02}/I_{01}. Since it has the shortest carbon chains so that there was less steric exclusion effect in the coordination procedure with rare earth ions, resulting in the structure was formed more easily and stable than the others. Besides, we selectively compared the luminescent quantum efficiency with those of some other ternary inorganic/organic hybrid materials [54]. It can be seen the former is lower than the latter in Ref. [54], which is easily to be understood. In the hybrid materials such as G–Si–Eu system, there does not exist the functional component for the effective energy absorption and energy transfer to Eu^{3+}, while it exist in the hybrid systems [54].

3.4. Ultraviolet–visible diffuse reflection absorption spectra

The ultraviolet–visible diffuse reflection absorption spectra of the hybrid materials are given in Fig. 4. The lines A, B, C, D, E and F denote the rare earth hybrid materials (A for G–Si–Tb, B for DG–Si–Tb, C for PG–Si–Tb, D for G–Si–Eu, E for DG–Si–Eu and F for PG–Si–Eu). It is observed that all the wide bands are located at about 270–340 nm in the line A, B, C and 275–360 nm in the line of D, E, F, which partially overlap with the fluorescence excitation spectra (wide bands at 280–360 nm in (a) and 350–450 nm in (b)). According to Dexter's exchange energy transfer theory [41], it can be primarily predicted that the energy gaps between the three precursors G–Si–RE, DG–Si–RE, PG–Si–RE and Tb^{3+} or Eu^{3+} are appropriate so that the precursors have absorbed abundant energy in ultro–visible extent to transfer the energy to the corresponding hybrid materials. Then the final hybrid materials can be expected

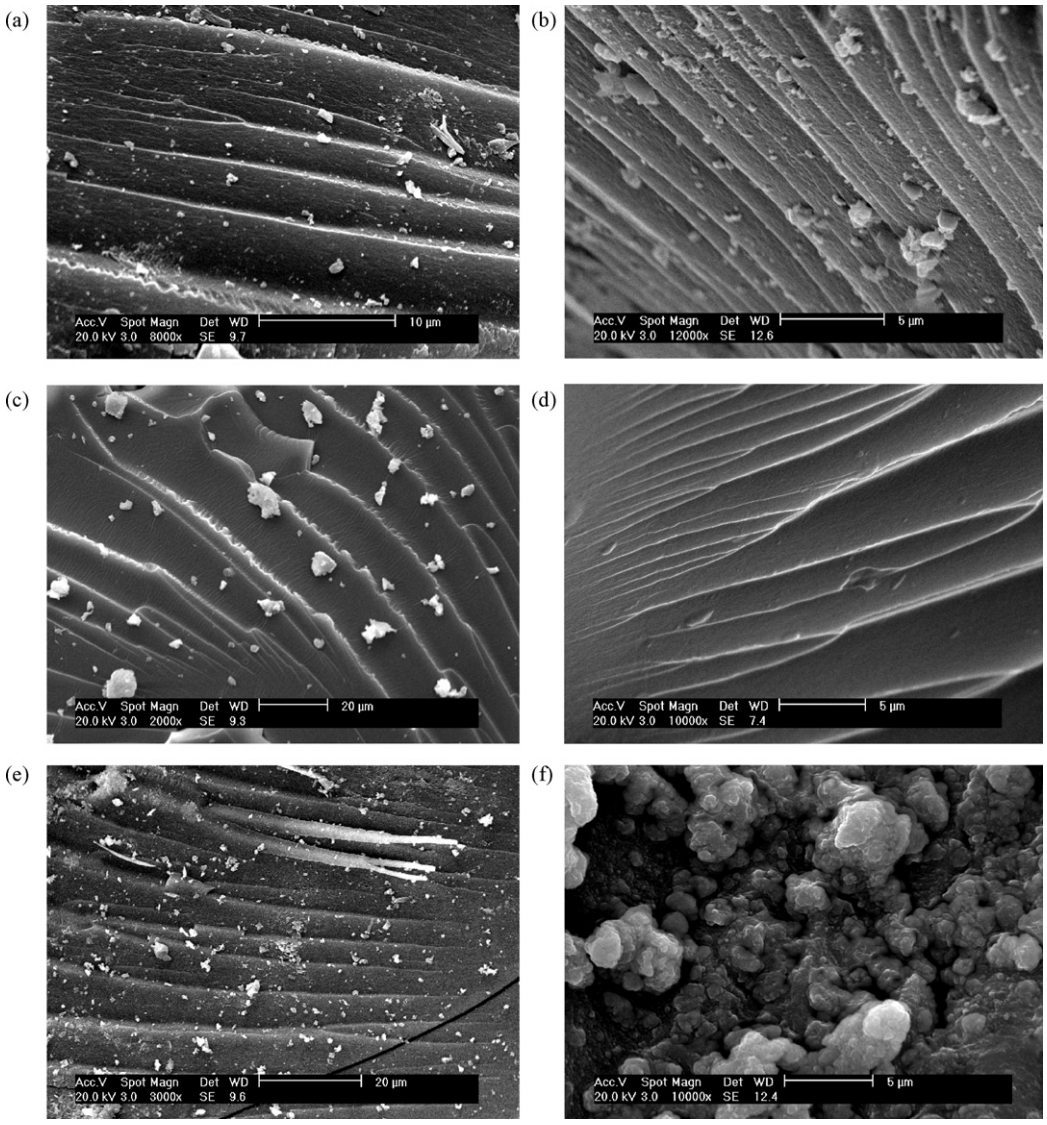

Fig. 5. SEM images of the hybrid materials (a) for G–Si–Tb, (b) for DG–Si–Tb, (c) for PG–Si–Tb (d) for G–Si–Eu, (e) for DG–Si–Eu and (f) for PG–Si–Eu.

to have strong luminescence after intramolecular energy transfer has accomplished, which is proved in the fluorescence spectra in Fig. 4. Moreover, these lines can be classified into two groups, and the shapes of each group are very similar, since each of them has the different rare earth metal center ions. Therefore, it is presumed that different structures of the rare earth hybrid materials arouse some difference in energy absorption in ultraviolet–visible extent, intramolecular energy transfer coefficient.

3.5. Scanning electron micrographs

The scanning electron micrographs for the six kinds of hybrid materials demonstrate that the homogeneous, molecular-based materials were obtained with strong covalent bonds bridging between the polymer and the inorganic matrix, which belongs to a complicated huge molecular system in nature (see Fig. 5). (a) G–Si–Tb, (b) G–Si–Eu, (c) DG–Si–Tb, (d) DG–Si–Eu, (e) PG–Si–Tb and (f) PG–Si–Eu. Compared with the hybrid material with doped lanthanide complexes generally experiencing the phase separation phenomena, in this paper the inorganic and organic phases can exhibit their distinct properties together in the hybrid materials we obtained containing covalent bonds [55].

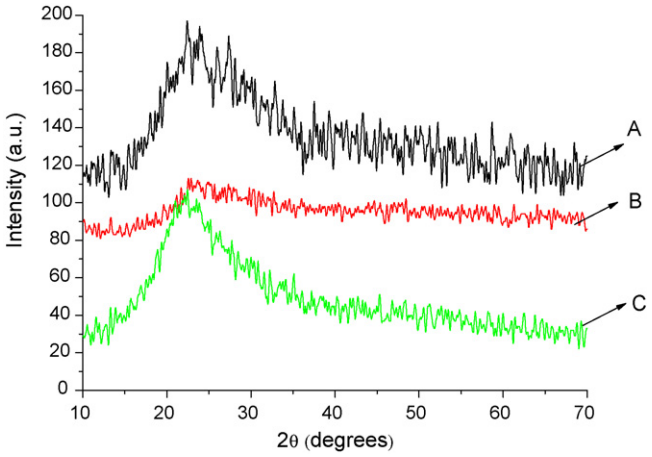

Fig. 6. The X-ray diffraction patterns for obtained hybrid materials A for G–Si–Eu, B for DG–Si–Eu and C for PG–Si–Eu.

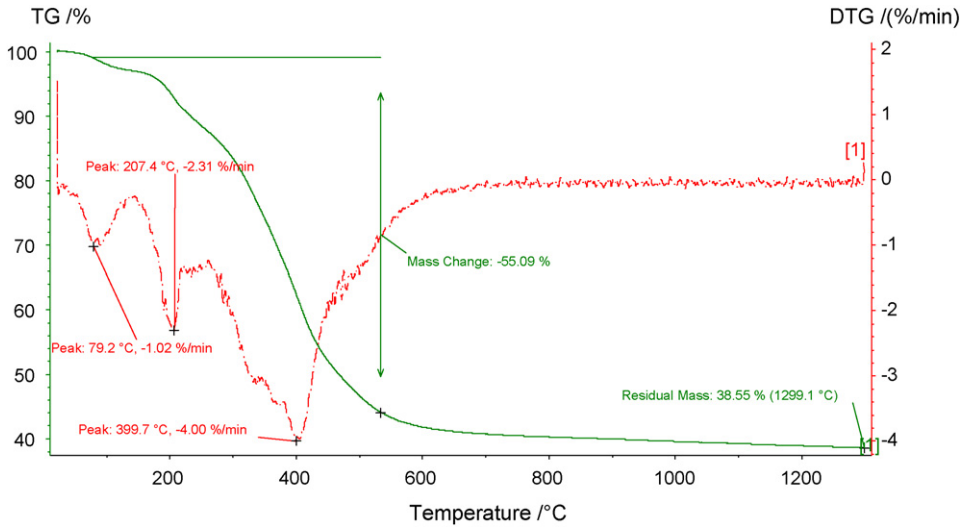

Fig. 7. The thermogravimetry trace (TG) and differential thermogravimetry trace (DTG) of the obtained hybrid materials DG–Si–Tb.

G–Si, DG–Si and PG–Si are the derivatives from glycol, diglycol and polyglycol and there exists no carboxyl groups in them. Therefore, its corresponding complex may be readily to form zero-dimensional chain-like polymeric structure and retain the coordinated position in corresponding bulk materials. However, when these lanthanide complex precursors coordinate to the rare earth metal ions, it is prone to form the zero-dimensional polymeric chains, which competes with the construction of a polymeric network structure of Si—O in hydrolysis/polycondensation process. Subsequently, it is seen from the micrographs that the tendency to form the polymeric network plays a primary role to result in the final structure and morphology: on the surfaces of each kind of these hybrid materials there exist the homogeneous bulk trunks or stripes of pine trees microstructure. The tiny phenomena attracting us is that there are some embranchments at the end of every trunk stripe and the stripes will continue to grow according to the directions of these embranchments, which forms the final structure as we see in the micrographs. Therefore, it is also indicated that the tendency to form the polymeric Si—O—Si network has become the primary tendency when it competed with the tendency to form one-dimensional chain-like structure. Ulteriorly, seen from Fig. 5f the material PG–Si–Eu presents the separate fragment but uniform blocks microstructure, and it is speculated that the polyglycol belongs to the polymer with long carbon chains which is different and its lanthanide complexes easily form the one-dimensional chain-like or two-dimensional layer polymeric structures, so the derivative may still keep this trend and result the final microstructure. Therefore, the different structures of the ligand or the change of center metal ions have played an important role in the microstructures of the lanthanide hybrid materials.

3.6. Powder XRD

The room-temperature X-ray diffraction patterns of the hybrid materials unfolded in Fig. 6 exhibit that the obtained hybrid materials are amorphous from 10° to 70°, (A) G–Si–Eu, (B) DG–Si–RE and (C) PG–Si–Eu. The broad peak centers on about 23.23° and 4.051 Å in Eu-containing hybrid material due to the amorphous siliceous backbone of the hybrids. The absence of any crystalline regions in these samples correlates with the presence of organic chains in the host inorganic framework. Moreover, it is illuminated that the polymeric chains of the polymer are essentially in a disordered order and the addition of the organic aromatic ligand into hybrid material results in an increase of the overall disorder of the siliceous skeleton, which brings the changes on conjugate systems of rare earth ions conforming to the conclusions obtained from the fluorescence spectra and SEM micrographs.

3.7. Thermogravimetric analysis

Fig. 7 shows the thermogravimetry trace (TG) and differential thermogravimetry trace (DTG) of DG–Si–Tb. Seen from the TG curve a, the hybrid material DG–Si–Tb has began to lost the mass at about 80 °C due to the loss of the residual organic solvent. And the hybrid mater has stopped losing the mass at about 545 °C, and during the temperature period from 80 °C to 545 °C the hybrid material DG–Si–Tb has lost about 55% of its mass. According to the structural molecule of the hybrid material DG–Si–Tb, the precursor DG–Si occupies four fifths (about 80%) in the mass of the D–Si–Tb, and it is illuminated that when the temperature has reached 200 °C, the DG–Si–Tb began to decompose with the falling off of DG–Si, while the temperature has reached 545 °C, the precursors DG–Si have not departed from the hybrid materials completely. Ulteriorly, it is indicated that the precursor DG–Si decomposed most quickly at about 400 °C seen from the DTG curve. Subsequently, the DG–Si–Tb retains the mass (about 40%) until 1300 °C without any decomposition or mass loss. It is concluded the hybrid material DG–Si–Tb possess the excellent thermal stability since the polymer ligand and the inorganic networks was induced into the hybrid materials with their inherent properties.

4. Conclusion

We have developed a novel and representative method for assembling the luminescent rare-earth molecular-based polymeric hybrid materials with strong chemical bonds, which contain the long organic polymeric carbon chains and organic network (Si–O–Si) in sol–gel process. The precursors G–Si, DG–Si and PG–Si were constructed by grafting 3-(triethoxysilyl)-propyl isocyanate on to diglycol and polyglycol, respectively, through the hydrogen transfer nucleophilic addition reaction between hydroxyl groups and the isocyanate groups. Then the rare earth coordination complex with functional polymers was synthesized after the coordination and hydrolysis and condensation processes. Furthermore, the photoluminescence properties, SEM diagraphs and thermogravimetric results illuminate that the hybrid materials

with different conjugated structures may have different effective intramolecular energy transfers, uniform microstructures, and thermodynamic stabilities. Therefore, these kinds of homogeneous molecular-based polymeric hybrid materials can be expected to have potential and significant application in optical and electronic devices in the future.

Acknowledgement

This work was supported by the National Natural Science Foundation of China (20671072).

References

[1] M. Elbanowshi, B. Makowska, J. Photochem. Photobiol. A: Chem. 99 (1996) 85–92.
[2] E. Soini, Trends Anal. Chem. 9 (1990) 90–93.
[3] J. Kido, H. Hayase, K. Hongawa, K. Nagai, K. Okuyama, Appl. Phys. Lett. 65 (1994) 2124–2126.
[4] N. Sabbatini, M. Guardigli, J.M. Lehn, Coord. Chem. Rev. 123 (1993) 201–228.
[5] Q.J. Zhang, P. Wang, X.F. Sun, Y. Zhai, P. Dai, Appl. Phys. Lett. 72 (1998) 407–409.
[6] R.J. Mears, L. Reekie, I.M. Jauncey, D.N. Payne, Electron. Lett. 22 (1986) 159–160.
[7] T. Suratwala, Z. Gardlund, K. Davidson, D.R. Uhlmann, Chem. Mater. 10 (1998) 190–198.
[8] C. Molina, K. Dahmouche, C.V. Santilli, Chem. Mater. 13 (2001) 2818–2823.
[9] B. Alpha, R. Ballardini, V. Balzani, J.M. Lehn, S. Perathoner, N. Sabbatini, Angew. Chem. Int. Ed. Engl. 26 (1987) 266–267.
[10] C. Sanchez, F. Ribot, New J. Chem. 18 (1994) 1007–1047.
[11] J.H. Harreld, A. Esaki, G.D. Stucky, Chem. Mater. 15 (2003) 3481–3489.
[12] P.N. Minoofar, R. Hernandez, S. Chia, B. Dunn, J.I. Zink, A.C. Franville, Am. Chem. Soc. 124 (2002) 14388–14396.
[13] J. Choi, R. Tamaki, S.G. Kim, R.M. Laine, Chem. Mater. 15 (1998) 3365–3375.
[14] A.C. Franville, D. Zambon, R. Mahiou, S. Chou, Y. Troin, J.C. Cousseins, J. Alloys Compd. 831 (1998) 275–277.
[15] A.C. Franville, R. Mahiou, D. Zambon, J.C. Cousseins, Solid State Sci. 3 (2001) 211–222.
[16] H.R. Li, J. Lin, H.J. Zhang, L.S. Fu, Chem. Mater. 14 (2002) 3651–3655.
[17] H.R. Li, J. Lin, H.J. Zhang, L.S. Fu, Chem. Commun. (2001) 1212–1213.
[18] Q.M. Wang, B. Yan, Inorg. Chem. Commun. 7 (2004) 747–750.
[19] D.W. Dong, S.C. Jiang, Y.F. Men, X.L. Ji, B.Z. Jiang, Adv. Mater. 12 (2000) 646–649.
[20] H.R. Li, L.S. Fu, H.J. Zhang, Thin Solid Films 416 (2002) 197–200.
[21] H.R. Li, J. Lin, L.S. Fu, J.F. Guo, Q.G. Meng, F.Y. Liu, H.J. Zhang, Micropor. Mesopor. Mater. 55 (2002) 103–107.
[22] F.Y. Liu, L.S. Fu, J. Wang, Z. Liu, H.R. Li, H.J. Zhang, Thin Solid Films 419 (2002) 178–182.
[23] K. Binnemans, P. Lenaerts, K. Driesen, C. Gorller-Walrand, J. Mater. Chem. 14 (2004) 191–195.
[24] A.C. Franville, D. Zambon, R. Mahiou, Chem. Mater. 12 (2000) 428–435.
[25] F.Y. Liu, L.S. Fu, H.J. Zhang, New J. Chem. 27 (2003) 233–235.
[26] M. Kawa, J.M. Frechet, J. Chem. Mater. 10 (1998) 286–296.
[27] H. Tanaka, J. Takahashi, J. Tsuchiya, J. Non-Cryst. Solids 109 (1989) 164–170.
[28] Y. Kubayashi, Y. Kurokuwa, Y. Imai, S. Muto, J. Non-Cryst. Solids 105 (1988) 198–200.
[29] T. Jin, S. Tsutsumi, Y. Deguchi, K. Machida, G. Adachi, J. Electrochem. Soc. 142 (1995) 195–197.
[30] M.A.B. Meador, E.F. Fabrizio, F. Ilhan, A. Dass, G.H. Zhang, P. Vassilaras, J.C. Johnston, N. Leventis, Chem. Mater. 17 (2005) 1085–1098.
[31] H. Chen, R.D. Archer, Macromolecules 29 (1996) 1957–1964.
[32] B.J. Gao, Y.F. Yang, Y. Cheng, D.J. Shi, Spectro. Spectra. Anal. 22 (2002) 371–374.
[33] V. Bekiari, G. Pistolis, P. Lianos, Chem. Mater. 11 (1999) 3189–3195.
[34] L.H. Wang, W. Wang, W.G. Zhang, E.T. Kang, W. Huang, Chem. Mater. 12 (2000) 2212–2218.
[35] J.R. MacCallum, C.A. Vincent (Eds.), Polymer Electrolyte Reviewss1, Elsevier Applied Science, London, 1987.
[36] R.G. Linford (Ed.), Electrochemical Science and Technology of Polymers 1, Elsevier Applied Science, London, 1987.
[37] F.M. Gray, Solid Polymer Electrolytes: Fundamentals and Technological Applications, VCH, New York, 1991.
[38] R.G. Linford (Ed.), Electrochemical Science and Technology of Polymers 2, Elsevier Applied Science, London, 1991.
[39] M.B. Armand, Adv. Mater. 2 (1990) 278–286.
[40] Y. Hasegawa, M. Yamamuro, Y. Wada, N. Kanehisa, Y. Kai, S. Yanagida, J. Phys. Chem. A 107 (2003) 1697–1702.
[41] D.L. Dexter, J. Chem. Phys. 21 (1953) 836–850.
[42] S. Sato, M. Wada, Bull. Chem. Soc. Jpn. 43 (1970) 1955–1962.
[43] T.D. Brown, T.M. Shepherd, J. Chem. Soc., Dalton Trans. (1973) 336–341.
[44] P.C.R. Soares-Santos, H.I.S. Nogueira, V. Félix, M.G.B. Drew, R.A.S. Ferreira, L.D. Carlos, T. Trindade, Chem. Mater. 15 (2003) 100–108.
[45] E.S. Teotonio, J.G.P. Espínola, H.F. Brito, O.L. Malta, S.F. Oliveria, D.L.A. de Foria, C.M.S. Izumi, Polyhedron 21 (2002) 1837–1844.
[46] L.D. Carlos, Y. Messaddeq, H.F. Brito, R.A.S. Ferreira, V.D. Bermudez, S.J.L. Ribeiro, Adv. Mater. 12 (2000) 594–598.
[47] M.F. Hazenkamp, G. Blasse, Chem. Mater. 2 (1990) 105–110.
[48] M.H.V. Werts, R.T.F. Jukes, J.W. Verhoeven, Phys. Chem. Chem. Phys. 4 (2002) 1542–1548.
[49] O.L. Malta, H.F. Brito, J.F.S. Menezes, F.R.G.E. Silva, S. Alves, F.S. Farias, A.V.M. daAndrade, J. Lumin. 75 (1997) 255–268.
[50] G.F. de Sa, O.L. Malta, C.D. Donega, A.M. Simas, R.L. Longo, P.A. Santa-Cruz, E.F. da Silva, Coord. Chem. Rev. 196 (2000) 165–195.
[51] J.C. Boyer, F. Vetrone, J.A. Capobianco, A. Speghini, M. Bettinelli, J. Phys. Chem. B 108 (2004) 20137–20143.
[52] C.A. Kodaira, A. Claudia, H.F. Brito, M.C.F.C. Felinto, J. Solid State Chem. 171 (2003) 401–407.
[53] K. Binnemans, K. Van Herck, C. Gorller-Walrand, Chem. Phys. Lett. 266 (1997) 297–302.
[54] B. Yan, X.F. Qiao, J. Phys. Chem. B 111 (2007) 12362–12374.
[55] R.A.S. Ferreira, L.D. Carlos, R.R. Goncalves, S.G.L. Ribeiro, V.D. Bermudez, Chem. Mater. 13 (2001) 2991–2998.